ADVANCING EARTH AND SPACE SCIENCE

JGR Oceans

RESEARCH ARTICLE

10.1029/2021JC018188

The Role of the Irminger Current in the Irminger Sea Northward Transport Variability

Nora Fried[1] and M. Femke de Jong[1]

[1]Department of Ocean Systems, NIOZ, Royal Netherlands Institute for Sea Research, Texel, The Netherlands

Key Points:

- The Irminger Current (IC) is a major contributor to the northward volume transport in the Irminger Sea
- The IC's volume transport decreased from 1993 to 2011 followed by an increase from 2012 to 2020
- Basin-wide to local changes in the density field contribute to transport variability at different time scales

Correspondence to:

N. Fried,
nora.fried@nioz.nl

Citation:

Fried, N., & de Jong, M. F. (2022). The role of the Irminger Current in the Irminger Sea northward transport variability. *Journal of Geophysical Research: Oceans*, *127*, e2021JC018188. https://doi.org/10.1029/2021JC018188

Received 28 OCT 2021
Accepted 2 FEB 2022

Abstract The Irminger Current (IC) on the western flank of the Reykjanes Ridge is an important contributor to the northward transport in the Atlantic Meridional Overturning Circulation. Here, we combine 28 years of Copernicus Marine Environment Monitoring Service (CMEMS) ocean reanalysis data with 6 years of mooring data to investigate variability in volume transport of the IC. We found a mean volume transport for the IC of 11.6 Sv between 1993 and 2020 revealing the dominance of the IC in the total Irminger Sea northward volume transport (20.3 Sv). We found a significant decrease (−3.7 Sv) in volume transport of the IC until 2011 followed by a steeper (but shorter, leading to +2.7 Sv) increase until 2020. These changes across the Irminger Sea section are dominated by the IC, which in turn are driven by changes in the density gradient across the Irminger Sea related to convection. On decadal and interannual time scales the IC volume transport is well correlated with the decrease in the sea surface height difference over the basin. In 2019, a temporary intensification of the western IC core led to an exceptionally strong volume transport of the IC with 20 Sv. This was caused by density changes within the IC boundaries due to the presence of mesoscale eddies. Thus, IC transport variability is a superposition of basin-wide to local processes that influence the velocity field on different time scales.

Plain Language Summary The Irminger Current (IC) transports relatively warm and saline water northwards along the Mid Atlantic Ridge toward Iceland, where one part continues further north and the rest turns around to flow south along Greenland. We investigate changes in the IC's northward transport using a combination of direct observations from moorings and a longer reanalysis time series. We found that the IC is dominating the northward volume transport in the eastern Irminger Sea. The IC is also driving the long-term decrease in the total northward volume transport. Its intensity depends on changes in the basin-wide density gradient between sea surface height (SSH) minimum in the convection area of the central Irminger Sea and the SSH maximum on top of the Mid Atlantic Ridge. This study shows that the high variability in transport can be explained by a combination of processes acting on different time scales. Changes in the IC and the central Irminger Sea are crucial to help us monitor changes in the overturning of the eastern subpolar North Atlantic.

1. Introduction

The Atlantic Meridional Overturning Circulation (AMOC) is one of the key components in the world's climate. Deep convection is an important process that contributes to overturning. In the North Atlantic, deep convection is found specifically in the Labrador and Irminger Sea (e.g., Lazier, 1973; Lazier et al., 2001; Marshall & Schott, 1999; Pickart et al., 2003, Pickart and Spall, 2007) and in the Nordic Seas (e.g., Eldevik et al., 2005; Messias et al., 2008; Våge et al., 2015). Deep convection in the Irminger Sea was first observed by Nansen in 1912 followed by more observations in recent years (de Jong et al., 2018, 2012; de Jong & de Steur, 2016; Pickart et al., 2003; Piron et al., 2017, 2015; Sverdrup et al., 1942; Våge et al., 2008). In a changing climate, the predicted increase in stratification in these regions can weaken or inhibit deep convection, resulting in a weakening of the AMOC (Eden & Willebrand, 2001; Sévellec et al., 2017; Spall & Pickart, 2001; Thomas et al., 2015).

The subpolar North Atlantic hydrography has been monitored with regular repeats of the World Ocean Circulation Experiment A01 E section (van Aken et al., 2011) and the Greenland to Portugal OVIDE section (Observatoire de la Variabilité Interannuelle à Décennale; Lherminier et al., 2007; Mercier et al., 2015). Since 2014, the AMOC strength in the subpolar North Atlantic has been measured continuously within the Overturning in the Subpolar North Atlantic Program (OSNAP, Li et al., 2021; Lozier et al., 2017, 2019). In the Irminger Sea, the OSNAP array aligns with the hydrographical sections observed nearly annually since 1990 (van Aken et al., 2011). Results from OSNAP show that most of the variability in overturning in the subpolar gyre (SPG) originates from the Irminger Sea and Iceland Basin (OSNAP East, Li et al., 2021; Lozier et al., 2019; Petit et al., 2020).

Therefore, the Irminger Sea is receiving increased attention as an area of interest in the connection between deep convection and transport variability. Here, we focus on the Irminger Current (IC) which contributes to the AMOC in the SPG and is located on the western side of the Reykjanes Ridge (RR, Figure 1a). The IC flows cyclonically around the Irminger Sea (Krauss, 1995; Reverdin et al., 2003) and continues southward off the East Greenland shelf along the East Greenland Current (EGC, Figure 1a). After rounding Cape Farewell, the IC joins the EGC and becomes the West Greenland Current (Cuny et al., 2002; de Jong et al., 2014).

The central Irminger Sea is the center of the cyclonic flow described above and the main area for convection in the Irminger Sea (de Jong & de Steur, 2016; de Jong et al., 2012; de Jong et al., 2018).

Various different water masses take part in the circulation described above. In the lower layers the IC transports North East Atlantic Deep Water (NEADW). The NEADW is a modified version of Iceland-Scotland Overflow Water (ISOW, Dickson et al., 2002; Racapé et al., 2019; Yashayaev, 2007) and contributes to the AMOC's lower limb with a density lower than the Denmark Strait Overflow Water, which flows down from the sill in the Denmark Strait (Macrander et al., 2005; Swift et al., 1980), and higher than the Labrador Sea Water (LSW, Lavender et al., 2005; Spall & Pickart, 2003; Våge et al., 2011) found in the central Irminger Sea. The NEADW was thought to reach the Irminger Sea through Charlie-Gibbs-Fracture-Zone (CGFZ) and the Bight Fracture Zone (BFZ) as major pathways, but more recent studies highlight the importance of smaller fracture zones along the ridge further north (Koman et al., 2020; Petit et al., 2018, 2019). In these fracture zones the ISOW entrains the overlying LSW, thus the NEADW becomes less saline and less dense than its source water.

In the upper layers the IC transports buoyant, warm and saline Irminger Subpolar Mode Water (SPMW, Garcia-Ibanez et al., 2015) northwards. The SPMW originates from the North Atlantic Current (NAC; Brambilla & Talley, 2008). SPMW is steered to Irminger Sea from the East Reykjanes Ridge Current through multiple gaps across the RR (Petit et al., 2019). The upper to intermediate water masses in the central Irminger Sea are modified by deep convection (de Jong & de Steur, 2016; de Jong et al., 2012; van Aken et al., 2011) and are therefore colder and fresher, contrasting with the warmer, more saline IC over the RR.

The IC has been described in various studies, most recently by de Jong et al. (2020). They presented mooring data from 2014 to 2016, which were the first year-round measurements of the IC. In the mean, the current consists of two surface-intensified cores flowing northward along the western flank of the RR with a weak southward return flow in between at intermediate depth (Figure 1b; de Jong et al., 2020; Petit et al., 2019; Våge et al., 2011). The eastern near-surface core is warmer and more saline than the western core (de Jong et al., 2020; Petit et al., 2019; Våge et al., 2011).

Previous estimates of volume transport vary between 8.5 and 19 Sv (1 Sv = 10^6 m^3 s^{-1}). A wide spectrum of different types and coverage of measurements, defined current boundaries and time frames likely contributed to this large range in transport (Chafik et al., 2014; Daniault et al., 2016; Sarafanov et al., 2012; Våge et al., 2011). The first full water column, year-round study of de Jong et al. (2020) narrows down the mean volume transport of the IC to 10.6 $\pm$ 9.2 Sv between 2014 and 2016. The high standard deviation highlights the strong temporal variability of the IC, which is likely the result of mesoscale activity first mentioned by Volkov (2005). More recently, Fan et al. (2013) showed that the RR is a region of increased eddy kinetic energy in the Irminger Sea. The strong temporal variability may also have contributed to the large range in previous transport estimates.

This study aims to get more insight into the interannual and decadal transport variability in the Irminger Sea using ocean reanalysis (1993–2020), mooring (2014–2020) and altimetry (1993–2020) data. We will focus on how changes in hydrography influenced the northward volume transport in the basin east of the convection region and the IC specifically. This paper is structured as follows. The data sets and methods used in this study are presented in Section 2. The results of the analysis are presented in Section 3. After a description of the reference, or mean state, we describe the long-term trends followed by the interannual variability and their relation to basin wide changes. Section 3 concludes with an analysis of a strong peak in IC transport observed by the mooring array in recent years. In Section 4 we discuss these results and their implications for the AMOC variability in the subpolar North Atlantic.

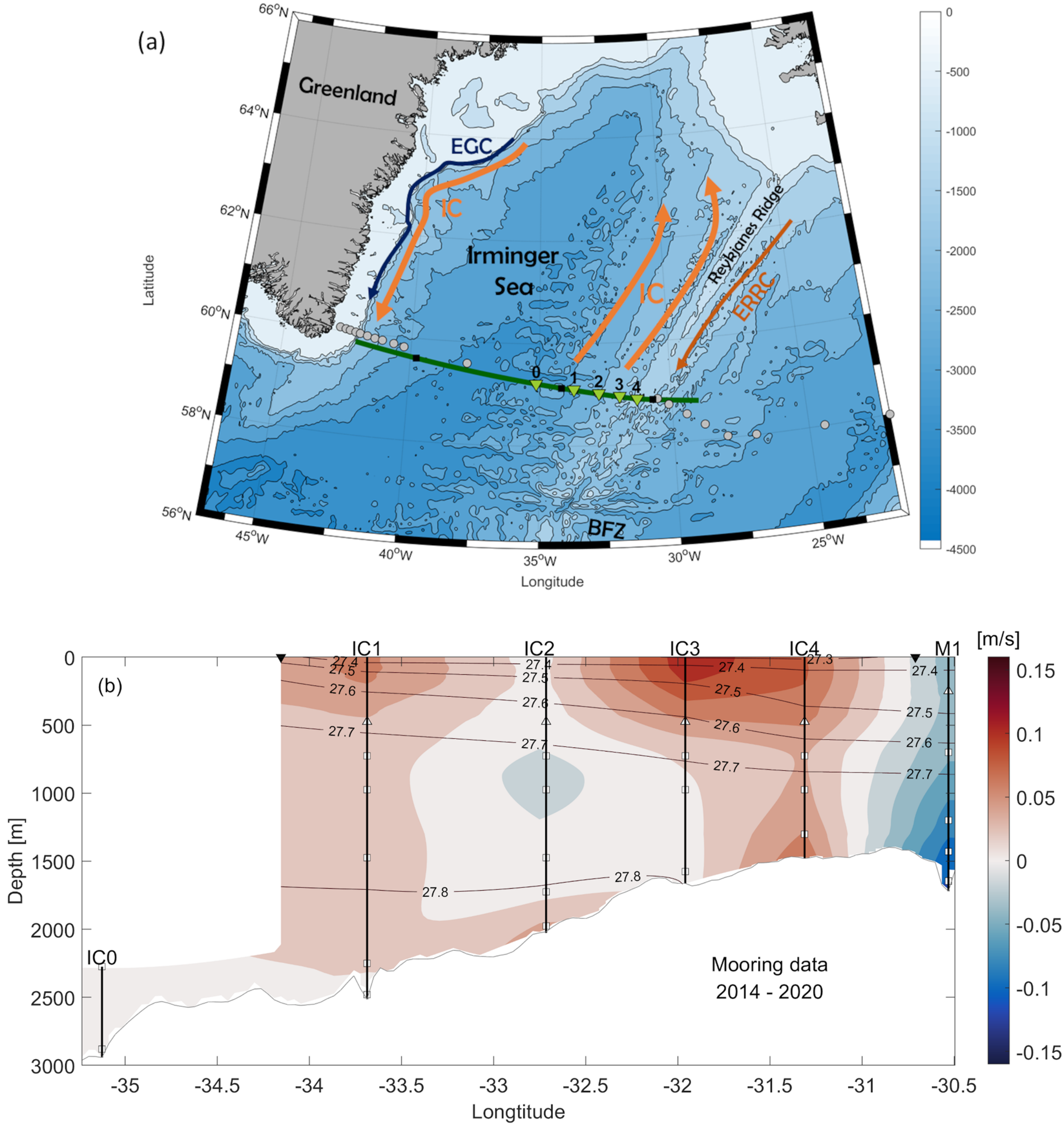

Figure 1. (a) Schematic of currents in the Irminger Sea with mooring locations indicated. Green triangles mark the Irminger Current (IC) moorings (IC0–IC4), gray circles represent overturning in the subpolar North Atlantic program east moorings, dark green line is the section of extracted reanalysis data. Indicated currents are the East Reykjanes Ridge Current (ERRC), the IC (two cores) and the East Greenland Current (EGC). The two topographic features are the Reykjanes Ridge (RR) and the Bight Fracture Zone (BFZ); black squares mark the transport boundaries (see Section 2.2) (b) velocities across IC mooring array from 2014 to 2020 with corresponding density field; vertical lines mark mooring positions with current meter (squares) and Acoustic Doppler Current Profiler (triangles) positions; red colors represent northward velocities and blue southward in (m/s). Gray line represents ridge topography.

2. Data and Methods

2.1. Data

2.1.1. Mooring Instrumentation and Data Processing

The Royal Netherlands Institute for Sea Research (NIOZ) mooring array consists of one short (IC0) and four long (IC1, IC2, IC3 and IC4) moorings located on the western side of the RR. They have been installed in July 2014 as part of the OSNAP array with the R/V Knorr and lastly recovered and redeployed with the R/V Pelagia in July 2020. These six years of observations are composed of four different deployments, initially two 1-year deployments (de Jong et al., 2020) followed by two 2-year deployments. In addition to the NIOZ moorings we included the nearby tall US OSNAP mooring (M1) on the eastern side of the RR. This additional mooring allows us to determine the boundary between the southward flowing East Reykjanes Ridge Current and the northward flowing IC.

The four long IC moorings are equipped with Sea-Bird Electronics SBE37 (MicroCATs) and Sea-Bird Electronics SBE56 (thermistors) to measure temperature and salinity. Velocities are measured by upward looking Acoustic Doppler Current Profilers (ADCPs) (RDI 75 kHz Long Ranger ADCP) and single-point current meters (either Aanderaa RCM11 or Nortek Aquadopps). The short IC mooring is equipped with MicroCATs and RCM11s. The US M1 mooring is equipped with an upward-looking ADCP, Nortek Aquadopp current meters and MicroCATs (Koman et al., 2020 for additional information).

The data were low-pass filtered by a 41-hr sixth-order Butterworth filter to remove tides and inertial motion and subsampled onto a daily grid. All fields were vertically interpolated using the MATLAB "pchip" function and horizontally interpolated linearly on a grid with bottom-following contours. The velocity data were rotated clockwise by 10° for along (V) and across (U) stream velocities along the RR.

Additional information on mooring data processing and interpolation methods are described in de Jong et al. (2020). For this analysis we use monthly means from the daily mooring data to better compare with the monthly reanalysis data.

The IC mooring array will be recovered and redeployed in summer 2022 for a new 2-year deployment.

2.1.2. Ocean Reanalysis and Altimetry Data

To investigate the long-term transport variability of the IC we analyzed the Copernicus Marine Environment Monitoring Services (CMEMS) global ocean physics reanalysis together with the analysis and forecast data (http://marine.copernicus.eu, E.U. Copernicus Marine Service Information). The CMEMS product from 1993 to 2020 has 1/12° horizontal resolution and 50 vertical levels. It uses the Nucleus for European Modelling of the Ocean (NEMO) model component and is forced at the surface by ECMWF ERA-Interim from 1993 to 2017 and then ERA5 reanalyses for recent years. We used the monthly output of reanalysis data from January 1993 to December 2019 and the analysis and forecast output onwards until August 2020. We use potential temperature, salinity, sea surface height (SSH), U, V and mixed layer depth (MLD).

The data were extracted around the OSNAP moorings (55–65°N, 45–25°W) and interpolated along the section between Greenland and the top of the RR (Figure 1a). The velocity data were rotated by 10°, similar to the mooring data, for along- and across-stream velocities along the RR.

The reanalysis data set was previously validated against the first 2 years of mooring data in de Jong et al. (2020).

We use the Ssalto/Duacs altimetry product from CMEMS from 1993 to 2020 to investigate the relationship between absolute dynamic topography (ADT) and volume transport with the 6-year mooring time series. We interpolate the altimetry data on the same section as the reanalysis data shown in Figure 1a. To investigate the mesoscale activity around the moorings we analyze fields of sea level anomaly (SLA) which is also measured by satellite altimetry.

2.2. Methods

We define the IC as being between 500 and 700 km distance to Cape Farewell as in Våge et al. (2011) (black triangles Figures 1b and 2, compare de Jong et al., 2020 for further explanations on transport boundaries). For

10.1029/2021JC018188

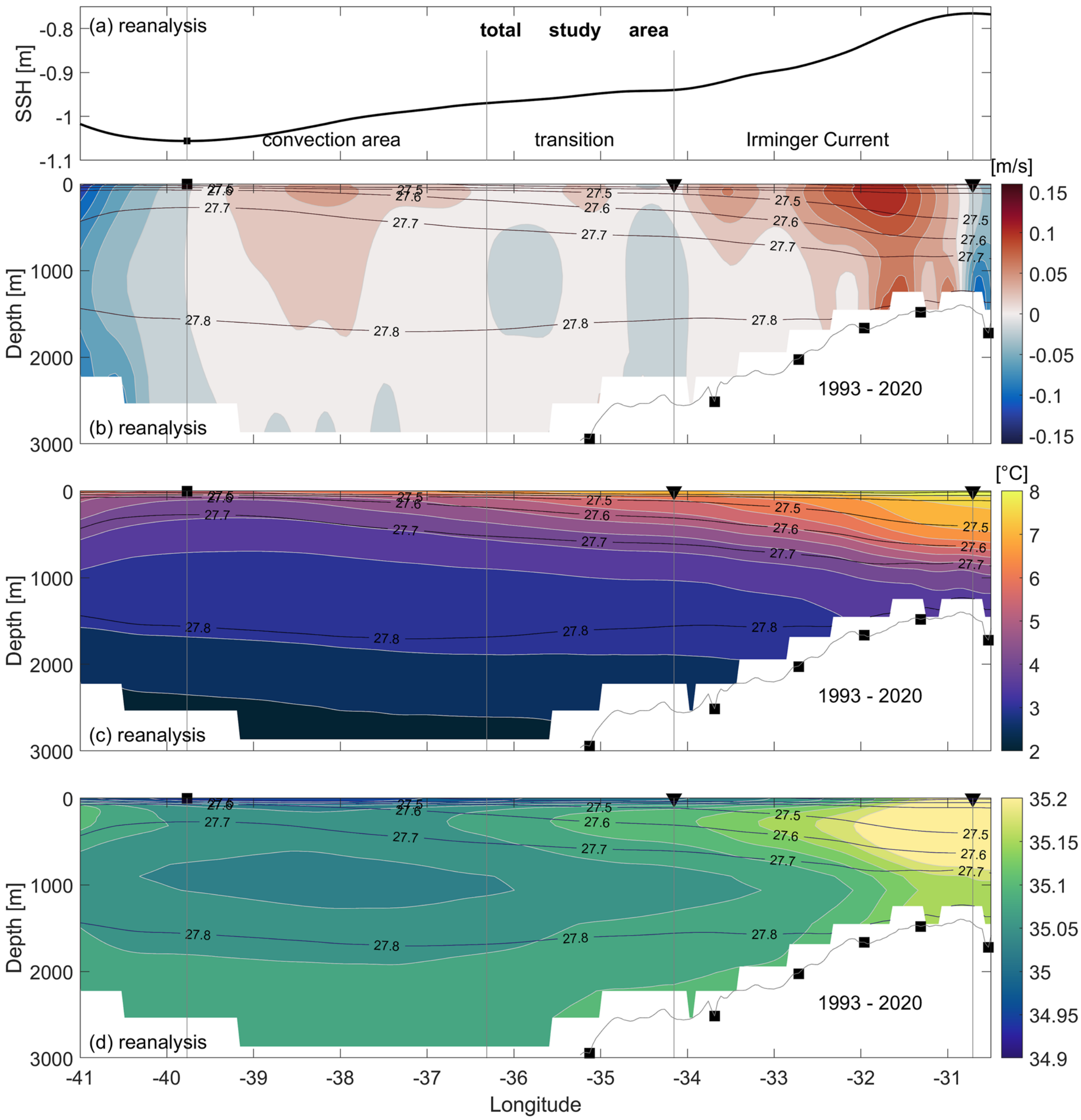

Figure 2. (a) Mean sea surface height (SSH) from 1993 to 2020 from reanalysis data across the Irminger Sea. Black marker shows SSH minimum in the central Irminger Sea. (b–d) mean section from 1993 to 2020 with mean isopycnals of across section velocity, conservative temperature and absolute salinity. Mooring locations are indicated along the depth contour with black boxes. Black markers and gray lines indicate boundaries for transport calculations (SSH minimum in the central Irminger Sea and 500–700 km off Cape Farewell with a transition zone).

transport computations on the reanalysis data we divide the Irminger Sea between the SSH minimum to the top of the RR into different regions (Figure 2a): The Irminger Current (500–700 km), the convection area (SSH minimum– −36.3°W), and a transition zone between the previous two. We determined the SSH minimum from the 28-year mean SSH across the Irminger Sea (black square Figure 2). The location of the minimum is stable over the 28-year time period.

From CMEMS and mooring data we calculated monthly and yearly mean volume transport. The volume transport is derived as

$$V(t) = \int_{X_w}^{X_e} \int_{\text{bottom}}^{\text{surface}} v(x, z, t) \; dz \; dx,$$

with X_e and X_w being the eastern and western boundary, respectively.

We calculated the yearly mean volume transport from July to June the following year to include a complete winter in each average and to better align with the mooring deployments and winter time convection. We thus have 27 yearly mean volume transport values.

We calculated the monthly maximum MLD in the Irminger Sea north of 58.5°N. For a yearly time series of maximum MLD we determined the maximum MLD between July and June for each year.

For an average conservative temperature of the upper water column in the study area (Figure 4b) we calculated a weighted average from the surface to 1450 m depth (depth of the top of the Reykjanes Ridge and the shallowest mooring).

3. Results

As a reference for the changes in the IC, we first look at the mean state in the Irminger Sea for the 28-year time period. Figure 2 shows the 1993–2020 mean velocity and hydrographic sections across the Irminger Sea extracted along the line shown in Figure 1a together with the mean SSH along that section. The hydrography is dominated by two main features, the cold, fresh convective water in the central Irminger Sea and the contrasting warmer, more saline water over the RR. Together, this creates a doming structure of the isopycnals and a cyclonic flow.

The circulation along the section is reflected in the mean SSH (Figure 2a). The SSH minimum in the central Irminger Sea is used as the western boundary defined to capture northward transport in the Irminger Sea. The strongest gradients in SSH are found between the IC boundaries. The second strongest gradient (approximately half as strong as over the IC) is associated with the doming isopycnals over the convective waters and is found between the boundaries of the convection area. We find the weakest gradient for the transition zone (only a quarter of the IC gradient). We will investigate the volume transport variability in the three separate regions: the IC, the convection area in the central Irminger Sea, the transition zone in between and their contribution to the total volume transport. We will refer to the total transport as "the section" (east of 39.8°W to the top of the ridge, gray lines Figure 2a).

Over the 28-year time period the total volume transport across the section was 20.3 ± 3.6 Sv (monthly standard deviation). The volume transport over the section is composed of 11.6 ± 3.2 Sv within the IC boundaries, 7.5 ± 3.6 Sv in the region defined as the convection area in the central Irminger Sea with 1.1 ± 3.4 Sv remaining for the transition area between both. The transition area is characterized by slow and opposing velocities. The IC is responsible for most of the volume transport but all areas contribute to the strong variability in the total northward transport. For the time period 2014–2016 good agreement was found between mooring and reanalysis data by de Jong et al. (2020) which also holds for the time period analyzed here (2014–2020, not shown). They found a mean IC transport of 10.6 ± 9.2 Sv (1.4 Sv std error) from mooring data and 10.7 ± 6.4 Sv from reanalysis data subsampled on mooring positions for the same time period. The higher standard deviation from the moorings is attributed to the higher temporal resolution of the mooring data. Here, we include results from the extended mooring time series from 2014 to 2020 in the comparison.

Looking at the IC in more detail, Figure 2b reveals the two-core structure with surface intensified velocities related to the steepening isopycnals. The eastern IC core shows higher velocities and is wider than the western core. The eastern IC core also shows a deeper extension at about 1500 m whereas the western core is mainly present at the surface. Over the top of the RR, the IC is confined by the southward flow of the East Reykjanes Ridge Current. The subsurface southward flow in between both cores (often called a recirculation in other studies) that is observed with the mooring array (Figure 1b) is not visible in the 28-year mean. Accordingly, reanalysis data might not be able to reproduce this.

Figures 2c and 2d show the mean sections of conservative temperature and absolute salinity over the 1993–2020 period. The two cores of the IC differ in terms of hydrographic properties (Figure 2c; de Jong et al., 2020). The eastern core is warmer and saltier than the western core due to its more direct link to the NAC shown by Petit et al. (2019). They found that the eastern core has a clear connection to the cross-ridge flow across the RR directly south of the array but also at the Bight Fracture Zone. The western core instead includes water that has been

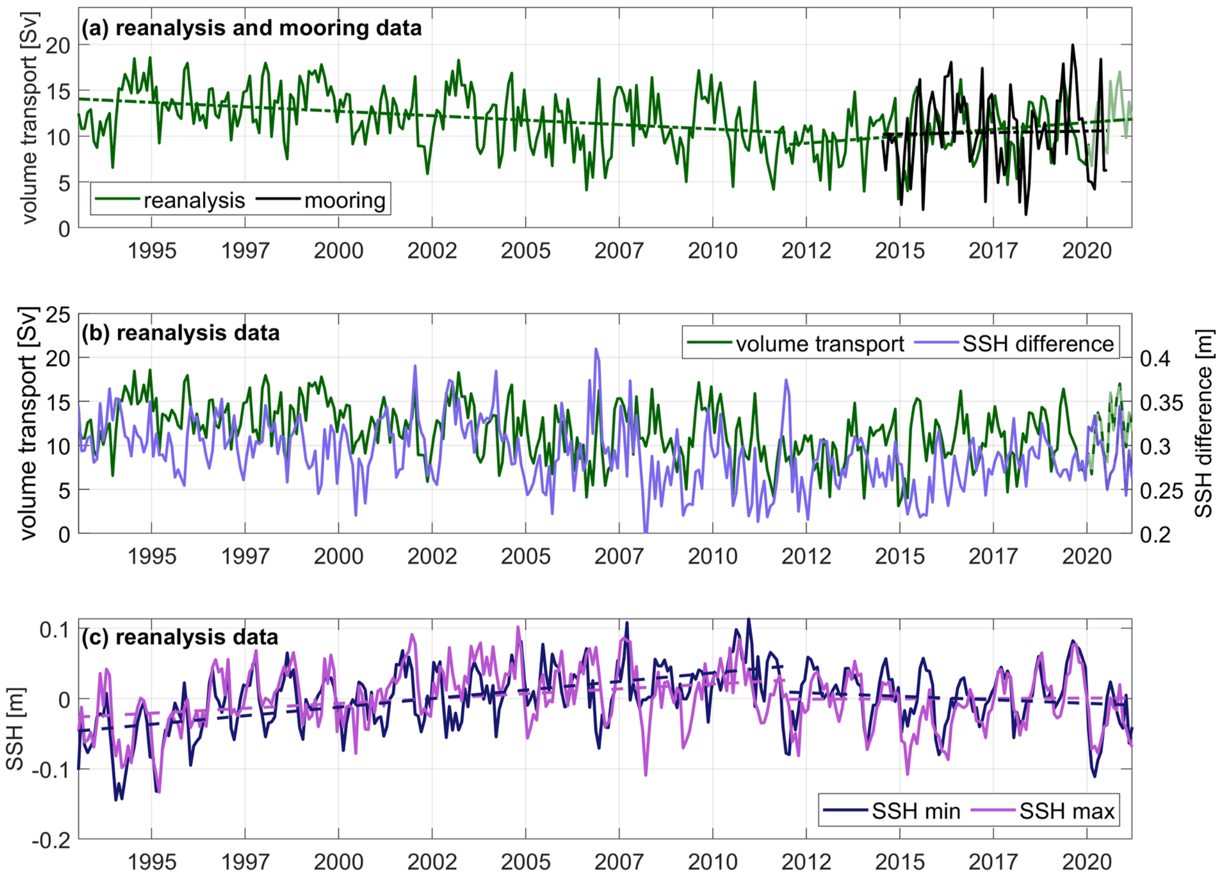

Figure 3. (a) Monthly volume transport of the Irminger Current (IC) from reanalysis data (green) with two separate trend lines from 1993 to 2011 and 2012–2020. Monthly mean mooring data is shown from 2014 to 2020 with respective trend line (black). The standard error for the mooring data is 0.83 Sv. (b) Monthly volume transport of the IC (500–700 km, green) from reanalysis data Copernicus Marine Environment Monitoring Service (CMEMS) from 1993 to 2020. sea surface height (SSH) difference between the SSH min and SSH max (700 km, purple, dashed line shows linear trend). Lighter colors in both panels present the forecast data from CMEMS. (c) Anomaly to mean monthly SSH (m) at SSH min in the convection area and SSH max on top of the ridge from 1993 to 2020; time series correspond to the SSH difference in (b).

modified while recirculating in the Irminger Sea. The variability in hydrographic properties in the Irminger Sea has been described in several studies (Sarafanov et al., 2012; Våge et al., 2011; van Aken et al., 2011). They found that the biggest changes in the water mass distribution are linked to periods of weak and strong convection. These changes are reflected in the SSH in the convection area, as shown by de Jong et al., 2012.

We will analyze the IC transport variability on decadal and interannual time scales in the following sections. In Section 3.4 we will focus on the implications for the mooring data with the example of a strong transport event in 2019.

3.1. Long-Term Trends in the Irminger Current Volume Transport

Here, we focus on the variability of the IC volume transport from the reanalysis data and compare it to the results from the mooring array to investigate long-term transport trends and drivers of variability.

Figure 3a shows the monthly volume transport over the full reanalysis time period (1993–2020) together with the volume transport observed by the mooring array from 2014 to 2020. The reanalysis time series shows a minimum around 2011–2012. To estimate long-term trends, we divided the time series into the period from 1993 to 2011 and 2012–2020. From 1993 to 2011, the reanalysis data reveals a statistically significant negative trend (95% confidence level) in volume transport of −3.7 Sv in total, or −0.2 Sv per year. From 2012 to 2020 there is

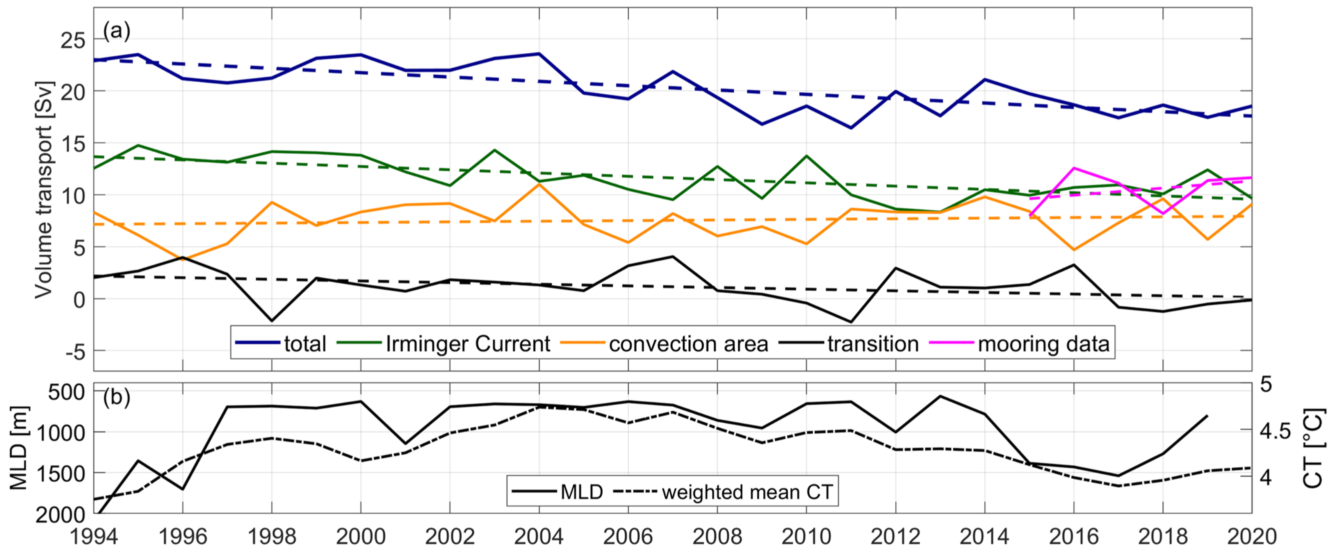

Figure 4. (a) Yearly mean volume transports for the Irminger Current (green), total transport across the Irminger Sea section (blue), convection area (orange) and the transition zone (black) from 1993 to 2020 for Copernicus Marine Environment Monitoring Service reanalysis data. Straight dashed lines indicate the linear trend. The yearly mean transport is calculated from July to June of the following year to include a full Winter. Yearly mean volume transport measured by the moorings from 2014 to 2020 is shown in pink. (b) Yearly maximum of mixed layer depth for the Irminger Sea from 1993 to 2019 (black, solid; left axis) and weighted mean conservative temperature for upper 1450 m along the section (black, dashed; right axis).

a significant increase of 2.7 Sv, or 0.3 Sv per year. This leads to a total decrease in volume transport of 2.2 Sv over the 1993–2020 period. Similar to the period from 2012 onwards in the reanalysis, the mooring data shows an increase, although less strong over this shorter period (0.3 Sv, or 0.05 Sv per year). Between 2014 and 2020 we found a mean IC transport of 10.4 ± 4.3 Sv from monthly mooring data with a standard error of 0.83 Sv.

Figure 3b shows the monthly reanalysis IC volume transport with the difference in SSH between the SSH minimum in the central Irminger Sea and the SSH maximum at the eastern boundary of the IC (black square and right triangle in Figure 2b). Here, we calculated a linear trend for the volume transport over the whole time period from 1993 to 2020 and found a significant decrease by −0.13 Sv per year (total −3.7 Sv). The trend in volume transport is mostly confined to the upper 1000 m and changes are stronger in the western core than in the eastern core (not shown).

We also found a significant decrease in the SSH difference between the SSH minimum in the central Irminger Sea and the eastern boundary on top of the ridge. Both time series are significantly, but weakly correlated ($r = 0.33$). In addition, we computed the SSH difference between the IC boundaries and found a stronger significant correlation with the IC volume transport of $r = 0.72$ ($r = 0.66$ for yearly mean values). The SSH difference between the IC boundaries also reveals a significant negative trend (not shown).

In Figure 3c we show the anomaly relative to the mean monthly SSH at the SSH minimum and maximum. They correspond to the SSH difference we show in Figure 3b. Both time series are significantly correlated by $r = 0.67$. We show the trend lines for the two time periods as in Figure 3a. The SSH maximum shows a weak positive trend whereas the SSH minimum in the convection area shows a somewhat stronger positive trend. The different strength in trends decreases the gradient between eastern and western boundary of the section and seems to be responsible for a decrease in volume transport of the IC between 1993 and 2011. Between 2012 and 2020, the trend is downward and again the trend in the SSH minimum is stronger than that observed in the SSH maximum. This large difference between SSH minimum and maximum is in turn responsible for the increase in volume transport.

3.2. Interannual Variability Along the Irminger Sea Section

We investigated changes in the yearly mean transport (Figure 4a) in three different regions in the Irminger Sea marked in Figure 2 with respect to the total transport.

The total volume transport over the Irminger Sea section shows a significant downward trend over the whole time period (−5.4 Sv total decrease). The IC is not only the biggest contributor to the total transport, but it is also the main cause of its long-term downward trend (−4.1 Sv comes from the decrease of the IC). The IC's interannual variability is also significantly correlated with the variability in total transport ($r = 0.6$, significant on 95% confidence level).

The convection area transport instead shows a slight positive increase of 0.8 Sv. The transition region transport shows a negative trend of −2.1 Sv, decreasing to around 0 Sv in 2020. Together both regions lead to a decrease in volume transport of −1.3 Sv and combined they are also correlated to the total transport ($r = 0.6$).

The yearly mean transport from the mooring data reveals a positive trend between 2014 and 2020 of 1.7 Sv which agrees with the trend we found for the IC from monthly data in Figure 3a.

3.3. Drivers for Long-Term Trends

The Irminger Sea is subject to periods of deep convection (de Jong et al., 2012; van Aken et al., 2011), which affects density gradients over the basin and thereby likely also the transports in the Irminger Gyre and IC. In addition to the volume transport Figure 4b shows the convective activity in the Irminger Sea illustrated by maximum MLD over each winter (from July to June of the next year). The early 1990's, as well as the years from 2015 to 2018, were years with deep (>1000 m) mixed layers in the Irminger Sea. The weighted mean average conservative temperature for the upper 1450 m of the Irminger Sea section (Figure 4b) shows a relatively cold basin in the 1990s, warming until the mid-2000s followed by cooling until 2017. Since 2017, temperatures are low but increasing slightly. This cooling and warming pattern mostly follows periods of strong (1990s, late 2000s to 2016) and weak convection. This implies that convective activity has an impact on the temperature in the Irminger Sea and accordingly changes gradients between the convection area and the eastern boundary of the IC. As we showed in Figure 3c changes are stronger at the SSH min in the convection area. We will investigate the changes in temperature along the section and the changes in SSH over the whole Irminger Sea in Figure 6.

We will look at density gradients across the Irminger Sea as a likely driver for transport variability through geostrophy. To elucidate basin wide changes in the density field, we focus on three time periods (Figure 5); the high transport period at the start of the record (1993–1995), the minimum (2011–2013) and the recent strong situation that overlaps with the mooring time period (2018–2020). We use 3-year means to smooth out smaller scale variability. Shown as well for these periods is the respective transport across the section, the density field and anomaly of the section velocity field with respect to the mean, and the IC density and velocity field. The early 1990's were characterized by strongly doming isopycnals in the central Irminger Sea, which created a strong density gradient across the IC and resulted in exceptionally strong velocities (Figures 5b and 5c). The eastern IC core was wider and deeper compared to the mean and the core of maximum velocities was shifted westward. In the 2011–2013 minimum transport period, the doming has been flattened out which resulted in a negative anomaly in velocities and weaker mean velocities (Figures 5d and 5e). At this time, both IC cores are clearly separated with a subsurface recirculation in between. The core with maximum velocities shifted eastward and was therefore closer to its mean position (compare Figure 2a). At the end of the record (2018–2020, Figure 5f), we again see a doming of the isopycnals with the strongest slope in the western part of the mooring array. This resulted in a stronger western IC core. The mean from 2018 to 2020 compares well with the mean section from the mooring array in Figure 1b.

All this together confirms that changes in the density structure of the Irminger Sea, related to periods of strong and weak convection (de Jong et al., 2012; van Aken et al., 2011), were responsible for changes in volume transport of the IC and across the Irminger Sea Section (Figure 5a). Changes do not only affect the section but are seen to occur over the whole Irminger Sea.

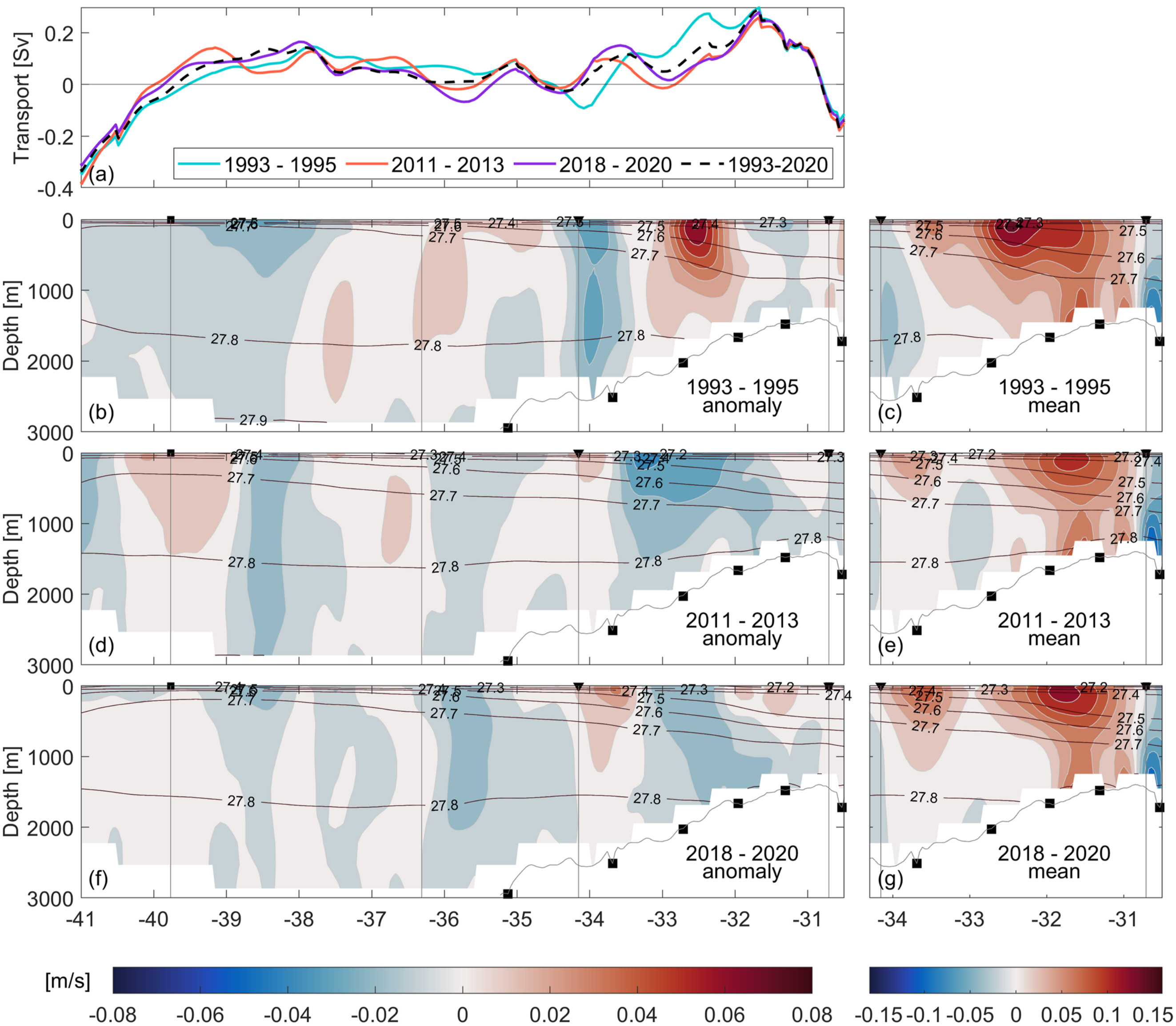

Figure 5. (a) Mean transport for 1993–1995 (cyan), 2011–2013 (red), 2018–2020 (purple) and total mean (1993–2020, dashed black) across the Irminger Sea. (b, d and f) velocity anomaly compared to long-term mean section of velocities with respective density field in contours for three time periods. One color level represents 0.01 m/s. (c, e and f) Mean velocity field for respective time period over Irminger Current. One color level represents 0.02 m/s. Black markers and gray lines indicate transport boundaries. Mooring locations are indicated along the depth contour with black squares.

To further investigate the density changes, we looked at conservative temperature and absolute salinity (not shown) in the respective three time periods. As seen in Figure 4b from the weighted mean conservative temperature the Irminger Sea experienced two periods. A warming until the middle of the record and a cooling after. Figures 6a–6c shows the anomalies to the mean field (shown in Figure 2) for conservative temperature with the corresponding density field. The periods 1993–1995 and 2018–2020 (Figures 6a and 6c) were characterized by anomalies in stratification whereas between 2011 and 2013 (Figure 6b) the horizontal temperature gradient has changed.

During the 1990's atmospheric conditions over the whole Irminger Sea were responsible for basin-wide cooling (van Aken et al., 2011). The early 1990's show the strongest cooling during the 28-year time period. This cooling is strongest at the surface down to a depth of 1500 m. The anomaly was strongest in the convection area and weakest in the IC. As a consequence, the temperature gradient increased which led to increased velocities

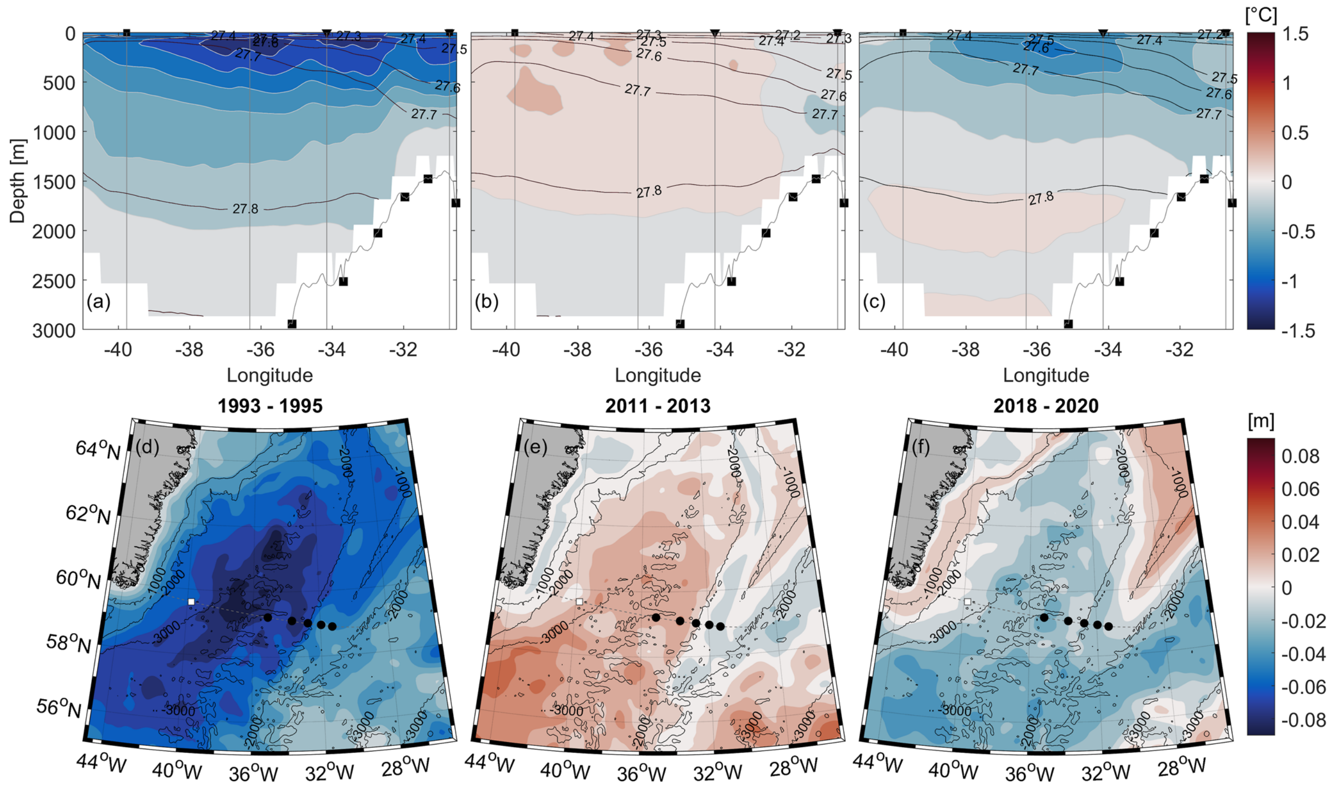

Figure 6. Anomalies compared to mean conservative temperature with averaged density field in contours for three respective time periods (a) 1993–1995, (b) 2011–2013 and (c) 2018–2020 from reanalysis data. Black markers and gray lines indicate transport boundaries. Mooring locations are indicated along the depth contour. One color level represents 0.2°C. (d–f) Sea surface height (SSH) anomalies to 1993–2020 mean SSH for respective time periods. Black dots indicate mooring locations. White square indicates the mean SSH minimum and gray dashed line the reanalysis section.

in the IC. Between 2018 and 2020 the surface to intermediate depth cooled down with the strongest cooling in the transition area. This resulted in a stronger density gradient and increased velocities especially in the western core (Figure 5g). At overflow water depth, below the 27.8-isopycnal, the temperature slightly increased. A more recent description of fluxes in the Irminger Sea related to convection can be found in de Jong et al. (2018) and Josey et al. (2019).

In contrast to that, during the time of minimum volume transport (2011–2013) the central Irminger Sea has warmed whereas the eastern core of the IC cooled. Similar changes can be seen in absolute salinity (not shown). This led to a reduced lateral density gradient between the IC cores. Isopycnals flattened out and led to reduced volume transport for the IC.

While changes during the first and last time period where nearly uniform for the whole basin, changes during 2011–2013 were different for the eastern core and the central Irminger Sea.

This is illustrated by maps of SSH anomaly for the three respective time periods shown in Figures 6d–6f. The 90's were characterized by strong basin-wide negative SSH anomalies compared to the 28-year mean, with a stronger SSH decrease around the SSH minimum and a weaker decrease over the top of the ridge (Figure 6d). This was responsible for an increase in the SSH gradient between the central Irminger Sea and the IC and resulted in strong transports. In contrast to that, the 2011–2013 period shows an increased SSH in the basin deeper than 2000 m, indicating restratification over the area of the basin where convective waters are found, and a weak decrease over shallower areas (Figure 6e). This contrast between the western convective waters and eastern Atlantic Waters in the 2010s is similar to that described for salinity by Fu et al. (2020). The opposing sign of the SSH anomaly between the central Irminger Sea and the ridge resulted in a reduced gradient and weaker transport. Between 2018 and 2020 SSH decreased again over the deep basin. This again led to stronger transport in the IC.

In summary, changes in temperature and salinity along the section that did not compensate in density changed the density gradient between the convection area and the IC. As a result, the volume transport of the IC changed following geostrophic transport balance.

3.4. Recent Changes at the IC Mooring Array

Over the period of the mooring observations (2014–2020), we investigate the absolute dynamic topography (ADT) from satellite altimetry. In reanalysis SSH and volume transport are necessarily coupled through the physics of the model which can lead to a higher correlation. In contrast to that, mooring observations and ADT are independent measurements at different sampling resolution. To investigate what those findings imply for the mooring array we show a similar analysis on the monthly mooring time series from 2014 to 2020 and focus on the strong transport event in 2019.

Figure 7a shows the monthly volume transport together with the ADT difference from altimetry data between 2014 and 2020. The volume transport shows a weak upward trend as already mentioned in Section 3.1. There is no trend in the ADT time series from 2014 to 2020. Between 2014 and 2020 ADT difference and volume transport from mooring data are significantly correlated with $r = 0.48$. Compared to the reanalysis data, where we correlated volume transport and SSH difference ($r = 0.72$), this correlation is weaker. But in contrast to reanalysis data where both variables are necessarily coupled through the physics of the model, the mooring data and ADT difference are independently measured on different sampling resolutions that can impact the correlation.

Notably the whole year of 2019 was characterized by strong volume transport. It was strongest during the second half of 2019 (Figure 7a) where the transport exceeded the mean transport for six consecutive months with a maximum volume transport in August 2019 of 20 Sv (nearly double the mean transport of 10.4 Sv). In the mean from 2014 to 2020 the volume transport was nearly equally distributed between western and eastern core (4.6 and 5.7 Sv respectively). In the 6-month average of 2019 the volume transport in the western core nearly doubled to 8.6 Sv while the eastern core decreased compared to the mean (5.5 Sv). We investigated the period of unusually strong volume transport in the second half of 2019 further by showing the month August as an example in Figures 7b–7d.

The ADT in August 2019 stands out from the mean (Figure 7b) because it had a stronger ADT gradient in the western IC core especially between IC1 and IC2. This is related to a steeper slope of the isopycnals in the western core, resulting in strong velocities (Figure 7c). Here, surface velocities increased by more than 0.2 m s^{-1}, while the eastern core increased by 0.12 m s^{-1}. In contrast to that, velocities at IC2 decreased by 0.1 m s^{-1}. The density difference over the western core arose due to warm anomaly between IC1 and IC2 which led to a local increase in the density difference (not shown). In consequence this strengthened velocities in the western core and increased the total volume transport. The density and velocity structure correspond with the signal of an anticyclone. Thus, we suggest that mesoscale variability is responsible for the strong changes in transport in 2019.

The anticyclone is visible in the sea level anomaly (SLA) map for August 2019 in Figure 7d. The (somewhat elongated) SLA maximum of the anticyclone is located between IC1 and IC2. The elongation could be due to averaging in time while the anticyclone is advected northward in the IC. The positive SLA is present for all months in 2019 that show increased transport and seems to travel northeastward together with the direction of the mean flow. The SLA map also exhibits low SLA around IC3 and IC4. Together with the velocity and density field from the mooring array that corresponds to a cyclone east of the anticyclone.

In summary, we find significant correlation between ADT difference and volume transport from mooring observations between 2014 and 2020 which supports our findings from the reanalysis data. The mooring data shows that mesoscale variability within the IC array can directly influence the velocity structure of the IC itself and thereby the total volume transport of the Irminger Current.

4. Summary and Discussion

In this study we combined six years of mooring observations (2014–2020) with 28 years of CMEMS ocean reanalysis data (1993–2020) to investigate the long-term and interannual variability in volume transport in the Irminger Sea.

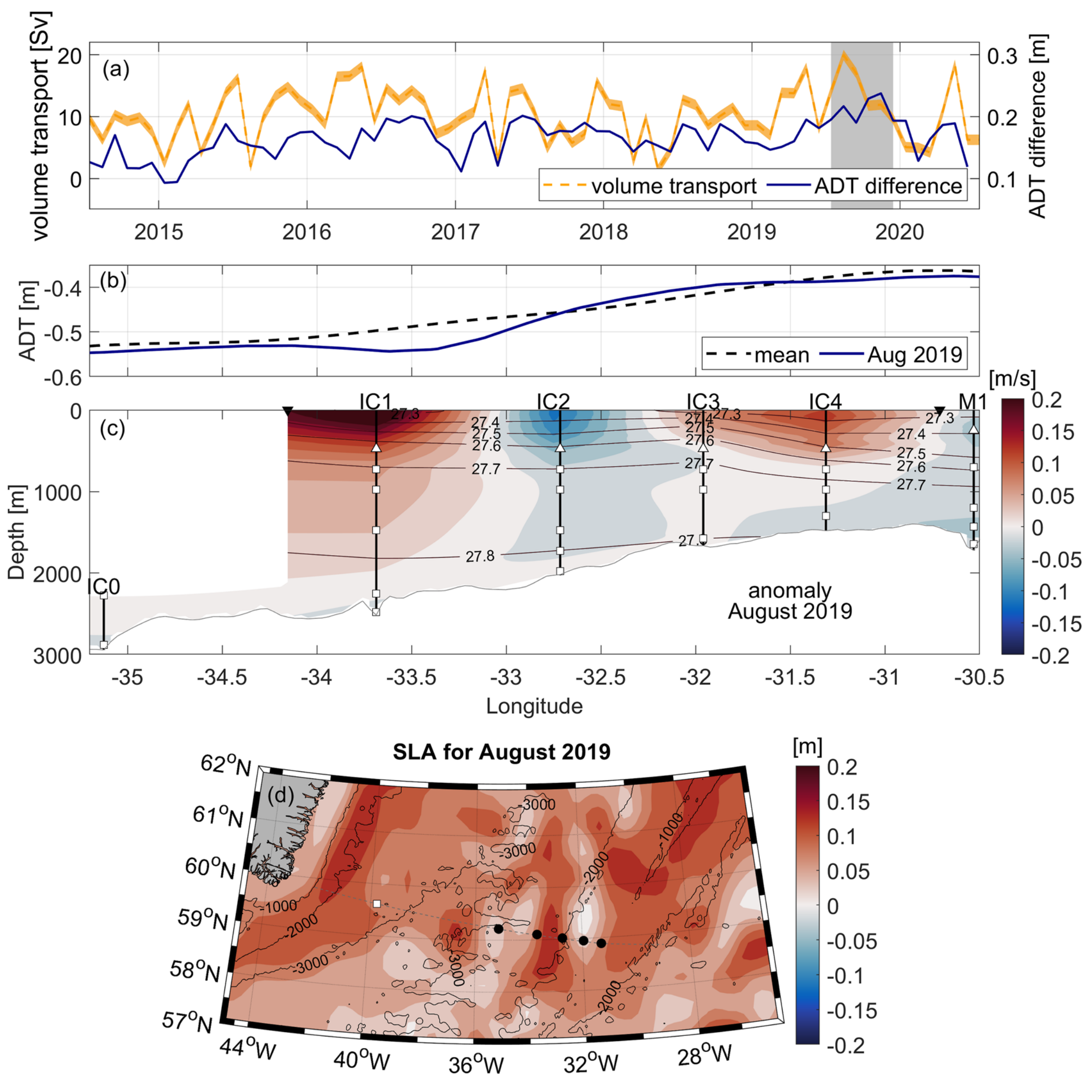

Figure 7. (a) Monthly volume transport (Sv) of the Irminger Current from mooring data between 2014 and 2020 (orange) with standard error as shading together with difference of absolute dynamic topography (ADT), (m), (blue) between Irminger Current boundaries; gray shading marks the period of strong transport in 2019 (b) mean ADT for 2014–2020 (dashed) and August 2019 (blue); (c) anomaly velocity field compared to the 2018–2020 mean with respective mean density field for 2018–2020. Vertical lines mark mooring positions with current meter and Acoustic Doppler Current Profiler positions. (d) Sea level anomaly, (m) for August 2019 from satellite altimetry. Black dots indicate mooring locations. White square indicates the mean sea surface height minimum and gray dashed line the reanalysis section.

We found that the IC contributes most (11.6 Sv) to the total northward volume transport of 20.3 Sv. For the convection area we found a mean northward transport of 7.5 Sv which compares well to an estimate from Våge et al. (2011) who found a mean transport of 6.8 ± 1.9 Sv for the convection area in a 17-year period. For the 28-year time period we found a decrease in the yearly volume transport across the section of −5.4 Sv (Figure 4a). The IC dominated this long-term trend in the total volume transport with a decrease of −4.1 Sv. More specifically, the IC transport decreased from 1993 to 2011 (0.2 Sv year^{-1}) followed by a slightly stronger (but shorter) increase from 2012 to 2020 (0.3 Sv year^{-1}, Figure 3a). This led to an overall negative trend in IC reanalysis volume transport from 1993 to 2020 of −0.13 Sv year^{-1}. The IC mooring array reveals a mean volume transport of 10.4 Sv, which compares well to previous estimates from de Jong et al. (2020) who reported a mean of 10.6 Sv between 2014 and 2016. In agreement with reanalysis data the IC mooring data showed a positive trend between 2014 and 2020 but with a weaker increase (0.05 Sv year^{-1}). The shorter-term variability from mooring and reanalysis data is similar.

The long-term trend in the IC volume transport is well correlated to the decrease in the SSH difference between the SSH minimum in the central Irminger Sea and the SSH maximum on top of the RR and even more to the SSH difference over the boundaries defining the IC. The decrease in the SSH difference is mainly driven by changes in the SSH minimum in the convection area. Strong convection events, as they occurred in the early 90's and in recent years, affected temperature and salinity basin-wide and led to a strengthened doming of isopycnals over the Irminger Sea (Figures 5 and 6; de Jong et al., 2018; Josey et al., 2019; van Aken et al., 2011). This is reflected in the increasing SSH difference. Accordingly, the density difference between the central Irminger Sea and the IC increased which resulted in increased velocities and volume transport in the IC. During the time of minimum volume transport (2011–2013) the eastern core over the RR cooled while the central Irminger Sea was warming. Accordingly, the density gradient decreased and the volume transport reached a minimum. In the 90's the uniform cooling over the whole Irminger Sea can be attributed to long-term temperature variations as a result of long-term variability in the net heat loss to the atmosphere (van Aken et al., 2011). This strong heat loss was triggered by consecutive and exceptionally severe winters. The (weaker) cooling up to 2018–2020 can also be attributed to convection forced by atmospheric cooling (de Jong et al., 2018; Josey et al., 2019). In contrast to that, the period from 2011 to 2013 was characterized by non-uniform changes across the Irminger Sea. The warming in the convection area is the result of slow restratification of the basin by warmer Atlantic waters. The heat gets advected from the IC to the central Irminger Sea.

We find statistically significant correlation between ADT difference and volume transport from the 2014–2020 mooring data of $r = 0.48$. The IC transport in the second half of 2019 was exceptionally high (20 Sv, nearly double the mean of 10.4 Sv between 2014 and 2020) and was related to an increased density gradient within the IC. With the month August 2019 we show that the IC volume transport was influenced by the presence of mesoscale eddies. This is supported by the mooring observations and the SLA maps. An anticyclone remained present for the months with strong volume transport and slowly propagated northward. The analysis of the SLA also reveals a cyclone just east of the anticyclone between the moorings IC3 and IC4. The area east of the RR is known as a region of high mesoscale activity (Fan et al., 2013; Volkov, 2005). Thus, IC transport variability is a superposition of basin-wide to local processes that influence the velocity field on different time scales.

Results from the OSNAP array showed that the overturning at OSNAP East is dominant in both overturning strength and variability (Li et al., 2021; Lozier et al., 2019), with 82% of the AMOC variability explained by OSNAP East. Li et al. (2021) looked in detail at the variability in OSNAP East over the 2014–2018 period and found that it was not explained by variability in the western boundary current but mainly originated from the interior Irminger Sea and Iceland Basin (Li et al., 2021). We find that transports in the interior Irminger Sea show long-term trends and interannual variability due to changes in the density field between the convective region and the RR. This agrees with Petit et al. (2020), who showed that water mass transformation occurring in the Irminger Sea, Iceland Basin and Nordic Seas is forced by local atmospheric buoyancy fluxes. However, we focused on changes in the northward volume transport in the Irminger Sea only. To investigate changes in the overturning both the northward transport in the east as well as the southward transport in the western Irminger Sea need to be considered on density levels. The strengthened doming of isopycnals in the central Irminger Sea is expected to lead to a similar transport increase to its west, which may compensate.

Nevertheless, changes in the IC and the central Irminger basin, as part of OSNAP East, are crucial to help us monitor changes in the AMOC in the eastern subpolar North Atlantic. Especially, considering the role of the IC in the overturning at different density levels in the AMOC will be subject of future studies.

Data Availability Statement

The following data sets were used in this study and are publicly available as: de Steur, L., and M.F. de Jong (2018). High-resolution current meter and hydrographic. Data from the Irminger Current mooring array 2014–2015. NIOZ Royal Netherlands Institute for Sea Research. Data set. https://doi.org/10.4121/uuid:77b2c4fc-c253-4494-91bd-8d1ef66a014a de Steur, L., and M.F. de Jong (2018). High-resolution current meter and hydrographic data from the Irminger Current mooring array 2015–2016. NIOZ Royal Netherlands Institute for Sea Research Institute for Sea Research. Data set. doi:10.4121/uuid:9ae97ceb-39e4-43ec-abdb-614103285c16. de Jong and Fried, 2021 de Jong, M. F., and N. Fried (2021). "High-resolution current meter and hydrographic data from the Irminger Current mooring array 2016–2018", doi: 10.25850/nioz/7b.b.nb de Jong and Fried, 2021 de Jong, M. F., and N. Fried (2021). "High-resolution current meter and hydrographic data from the Irminger Current mooring array 2018–2020", doi:10.25850/nioz/7b.b.pb we use CMEMS global ocean physics reanalysis together with the analysis and forecast data GLOBAL_REANALYSIS_PHY_001_030_monthly and GLOBAL_ANALYSIS_FORECAST_PHY_001_024_monthly respectively. We use the Ssalto/Duacs altimetry product from CMEMS SEALEVEL_GLO_PHY_L4_REP_OBSERVATIONS_008_047.

Acknowledgments
We acknowledge the fieldwork support provided by the officers, crews and technicians of the R/V Knorr, R/V Pelagia, RRS Discovery and the R/V Neil Armstrong. We thank W. E. Johns (University of Miami) for sharing the M1 data. This study has been conducted using E.U. Copernicus Marine Service Information. This project was funded by the European Union seventh Framework Program (FP7 2007–2013) under Grant 308299 (NACLIM) and the Horizon 2020 Research and Innovation Program under Grant 727852 (Blue-Action).

References

Brambilla, E., & Talley, L. D. (2008). Subpolar mode water in the northeastern Atlantic: 1. Averaged properties and mean circulation. *Journal of Geophysical Research*, *113*, C04025. https://doi.org/10.1029/2006JC004062

Chafik, L., Rossby, T., & Schrum, C. (2014). On the spatial structure and temporal variability of poleward transport between Scotland and Greenland. *Journal of Geophysical Research: Oceans*, *119*(2), 824–841. https://doi.org/10.1002/2013JC009287

Cuny, J., Rhines, P. B., Niiler, P. P., & Bacon, S. (2002). Labrador Sea boundary currents and the fate of the Irminger Sea water. *Journal of Physical Oceanography*, *32*(2), 627–647.

Daniault, N., Mercier, H., Lherminier, P., Sarafanov, A., Falina, A., & Zunino, P., et al. (2016). The northern North Atlantic Ocean mean circulation in the early 21st century. *Progress in Oceanography*, *146*, 142–158. https://doi.org/10.1016/j.pocean.2016.06.007

de Jong, M. F., Bower, A. S., & Furey, H. H. (2014). Two years of observations of warm-core anticyclones in the Labrador Sea and their seasonal cycle in heat and salt stratification. *Journal of Physical Oceanography*, *44*(2), 427–444. https://doi.org/10.1175/JPO-D-13-070.1

de Jong, M. F., & de Steur, L. (2016). Strong winter cooling over the Irminger Sea in winter 2014–2015, exceptional deep convection, and the emergence of anomalously low SST. *Geophysical Research Letters*, *43*, 7106–7113. https://doi.org/10.1002/2016GL069596

de Jong, M. F., de Steur, L., Fried, N., Bol, R., & Kritsotalakis, S. (2020). Year-round measurements of the Irminger Current: Variability of a two-core current system observed in 2014–2016. *Journal of Geophysical Research: Oceans*, *125*(10), e2020JC016193.

de Jong, M. F., Oltmanns, M., Karstensen, J., & de Steur, L. (2018). Deep convection in the Irminger Sea observed with a dense mooring array. *Oceanography*, *31*, 50–59. https://doi.org/10.5670/oceanog.2018.109

de Jong, M. F., van Aken, H. M., Våge, K., & Pickart, R. S. (2012). Convective mixing in the central Irminger Sea: 2002–2010. *Deep-Sea Research I*, *63*, 36–51. https://doi.org/10.1016/j.dsr.2012.01.003

Dickson, B., Yashayaev, I., Meincke, J., Turrell, B., Dye, S., & Holfort, J. (2002). Rapid freshening of the deep North Atlantic Ocean over the past four decades. *Nature*, *416*(6883), 832–837.

Eden, C., & Willebrand, J. (2001). Mechanism of interannual to decadal variability of the North Atlantic circulation. *Journal of Climate*, *14*(10), 2266–2280.

Eldevik, T., Straneo, F., Sandø, A. B., & Furevik, T. (2005). Pathways and export of Greenland Sea Water. In *The Nordic Seas: An integrated perspective*.

Fan, X., Send, U., Testor, P., Karstensen, J., & Lherminier, P. (2013). Observations of Irminger Sea anticyclonic eddies. *Journal of Physical Oceanography*, *43*(4), 805–823.

Fu, Y., Li, F., Karstensen, J., & Wang, C. (2020). A stable Atlantic meridional overturning circulation in a changing North Atlantic Ocean since the 1990s. *Science Advances*, *6*(48), eabc7836.

Garcia-Ibanez, M. I., Pardo, P. C., Carracedo, L. I., Mercier, H., Lherminier, P., Rios, A. F., & Perez, F. F. (2015). Structure, transports and transformations of the water masses in the Atlantic Subpolar Gyre. *Progress in Oceanography*, *135*, 18–36.

Josey, S. A., De Jong, M. F., Oltmanns, M., Moore, G. K., & Weller, R. A. (2019). Extreme variability in Irminger Sea Winter heat loss revealed by ocean observatories initiative mooring and the ERA5 reanalysis. *Geophysical Research Letters*, *46*(1), 293–302.

Koman, G., Johns, W. E., & Houk, A. (2020). Transport and evolution of the East Reykjanes Ridge current. *Journal of Geophysical Research: Oceans*, *125*(10), e2020JC016377.

Krauss, W. (1995). Currents and mixing in the Irminger Sea and in the Iceland basin. *Journal of Geophysical Research*, *100*(C6), 10851–10871.

Lavender, K. L., Owens, W. B., & Davis, R. E. (2005). The mid-depth circulation of the subpolar North Atlantic Ocean as measured by subsurface floats. *Deep Sea Research Part I: Oceanographic Research Papers*, *52*(5), 767–785.

Lazier, J., Pickart, R., & Rhines, P. (2001). Deep convection. *International Geophysics*, *77*, 387–400.

Lazier, J. R. (1973). The renewal of Labrador Sea water. *Deep Sea Research and oceanographic abstracts* (Vol. 20, pp. 341–353). Elsevier. 4.

Lherminier, P., Mercier, H., Gourcuff, C., Alvarez, M., Bacon, S., & Kermabon, C. (2007). Transports across the 2002 Greenland-Portugal Ovide section and comparison with 1997. *Journal of Geophysical Research*, *112*(C7).

Li, F., Lozier, M. S., Bacon, S., Bower, A. S., Cunningham, S. A., & de Jong, M. F., et al. (2021). Subpolar North Atlantic western boundary density anomalies and the meridional overturning circulation. *Nature Communications*, *12*(1), 1–9.

Lozier, M. S., Bacon, S., Bower, A. S., Cunningham, S. A., De Jong, M. F., & De Steur, L., et al. (2017). Overturning in the subpolar North Atlantic Program: A new international ocean observing system. *Bulletin of the American Meteorological Society*, *98*(4), 737–752. https://doi.org/10.1175/BAMS-D-16-0057.1

Lozier, M. S., Li, F., Bacon, S., Bahr, F., Bower, A. S., & Cunningham, S. A., et al. (2019). A sea change in our view of overturning in the subpolar North Atlantic. *Science*, *363*(6426), 516–521.

Macrander, A., Send, U., Valdimarsson, H., Jónsson, S., & Käse, R. H. (2005). Interannual changes in the overflow from the Nordic Seas into the Atlantic Ocean through Denmark Strait. *Geophysical Research Letters*, *32*(6).

Marshall, J., & Schott, F. (1999). Open-ocean convection: Observations, theory, and models. *Reviews of Geophysics*, *37*(1), 1–64.

Mercier, H., Lherminier, P., Sarafanov, A., Gaillard, F., Daniault, N., & Desbruyères, D., et al. (2015). Variability of the meridional overturning circulation at the Greenland–Portugal OVIDE section from 1993 to 2010. *Progress in Oceanography*, *132*, 250–261. https://doi.org/10.1016/j.pocean.2013.11.001

Messias, M. J., Watson, A. J., Johannessen, T., Oliver, K. I. C., Olsson, K. A., & Fogelqvist, E., et al. (2008). The Greenland sea tracer experiment 1996–2002: Horizontal mixing and transport of Greenland sea intermediate water. *Progress in Oceanography*, *78*(1), 85–105.

Petit, T., Lozier, M. S., Josey, S. A., & Cunningham, S. A. (2020). Atlantic deep water formation occurs primarily in the Iceland Basin and Irminger Sea by local buoyancy forcing. *Geophysical Research Letters*, *47*(22), e2020GL091028

Petit, T., Mercier, H., & Thierry, V. (2018). First direct estimates of volume and water mass transports across the Reykjanes Ridge. *Journal of Geophysical Research: Oceans*, *123*(9), 6703–6719. https://doi.org/10.1029/2018JC013999

Petit, T., Mercier, H., & Thierry, V. (2019). New insight into the formation and evolution of the East Reykjanes Ridge current and Irminger Current. *Journal of Geophysical Research: Oceans*, *124*(12), 9171–9189. https://doi.org/10.1029/2019JC015546

Pickart, R. S., & Spall, M. A. (2007). Impact of Labrador Sea convection on the North Atlantic meridional overturning circulation. *Journal of Physical Oceanography*, *37*(9), 2207–2227. https://doi.org/10.1175/JPO3178.1

Pickart, R. S., Straneo, F., & Moore, G. K. (2003). Is Labrador Sea water formed in the Irminger basin? *Deep Sea Research Part I: Oceanographic Research Papers*, *50*(1), 23–52.

Piron, A., Thierry, V., Mercier, H., & Caniaux, G. (2015). Observations of basin scale deep convection in the Irminger Sea with Argo floats in the Winter of 2011–2012. *Deep-Sea Research I*, *109*, 76–90. https://doi.org/10.1016/j.dsr.2015.12.012

Piron, A., Thierry, V., Mercier, H., & Caniaux, G. (2017). Gyre-scale deep convection in the subpolar North Atlantic Ocean during winter 2014–2015. *Geophysical Research Letters*, *44*, 1439–1447. https://doi.org/10.1002/2016GL071895

Racapé, V., Thierry, V., Mercier, H., & Cabanes, C. (2019). ISOW spreading and mixing as revealed by Deep-Argo floats launched in the Charlie-Gibbs fracture zone. *Journal of Geophysical Research: Oceans*, *124*(10), 6787–6808. https://doi.org/10.1029/2019JC015040

Reverdin, G., Niiler, P. P., & Valdimarsson, H. (2003). North Atlantic surface ocean currents. *Journal of Geophysical Research*, *108*(3002), 10–1029.

Sarafanov, A., Falina, A., Mercier, H., Sokov, A., Lherminier, P., & Gourcuff, C., et al. (2012). Mean full-depth summer circulation and transports at the northern periphery of the Atlantic Ocean in the 2000s. *Journal of Geophysical Research*, *117*(C1). https://doi.org/10.1029/2011JC007572

Sévellec, F., Fedorov, A. V., & Liu, W. (2017). Arctic Sea-ice decline weakens the Atlantic meridional overturning circulation. *Nature Climate Change*, *7*(8), 604–610. https://doi.org/10.1038/nclimate3353

Spall, M. A., & Pickart, R. S. (2001). Where does dense water sink? A subpolar gyre example. *Journal of Physical Oceanography*, *31*(3), 810–826.

Spall, M. A., & Pickart, R. S. (2003). Wind-driven recirculations and exchange in the Labrador and Irminger seas. *Journal of Physical Oceanography*, *33*(8), 1829–1845.

Sverdrup, H. U., Johnson, M. W., & Fleming, R. H. (1942). *The oceans: Their physics, chemistry, and general biology* (Vol. 1087). Prentice-Hall.

Swift, J. H., Aagaard, K., & Malmberg, S. A. (1980). The contribution of the Denmark Strait overflow to the deep North Atlantic. *Deep-Sea Research Part A. Oceanographic Research Papers*, *27*(1), 29–42.

Thomas, M. D., Tréguier, A. M., Blanke, B., Deshayes, J., & Voldoire, A. (2015). A Lagrangian method to isolate the impacts of mixed layer subduction on the meridional overturning circulation in a numerical model. *Journal of Climate*, *28*(19), 7503–7517. https://doi.org/10.1175/JCLI-D-14-00631.1

Våge, K., Moore, G. W. K., Jónsson, S., & Valdimarsson, H. (2015). Water mass transformation in the Iceland Sea. *Deep Sea Research Part I: Oceanographic Research Papers*, *101*, 98–109. https://doi.org/10.1016/j.dsr.2015.04.001

Våge, K., Pickart, R. S., Moore, G. W. K., & Ribergaard, M. H. (2008). Winter mixed layer development in the central Irminger Sea: The effect of strong, intermittent wind events. *Journal of Physical Oceanography*, *38*(3), 541–565. https://doi.org/10.1175/2007JPO3678.1

Våge, K., Pickart, R. S., Sarafanov, A., Knutsen, Ø., Mercier, H., & Lherminier, P., et al. (2011). The Irminger Gyre: Circulation, convection, and interannual variability. *Deep Sea Research Part I: Oceanographic Research Papers*, *58*(5), 590–614. https://doi.org/10.1016/j.dsr.2011.03.001

van Aken, H. M., de Jong, M. F., & Yashayaev, I. (2011). Decadal and multi-decadal variability of Labrador Sea Water in the north-western North Atlantic Ocean derived from tracer distributions: Heat budget, ventilation, and advection. *Deep Sea Research Part I: Oceanographic Research Papers*, *58*(5), 505–523.

Volkov, D. L. (2005). Interannual variability of the altimetry-derived eddy field and surface circulation in the extratropical North Atlantic Ocean in 1993–2001. *Journal of physical oceanography*, *35*(4), 405–426.

Yashayaev, I. (2007). Hydrographic changes in the Labrador Sea, 1960–2005. *Progress in Oceanography*, *73*(3–4), 242–276.